

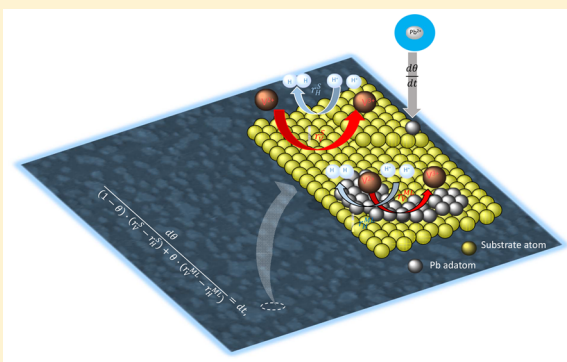
Electroless Deposition of Pb Monolayer: A New Process and Application to Surface Selective Atomic Layer Deposition

Dongjun Wu,[†] Dhairat J. Solanki,[†] J. Luis Ramirez,[†] Wenli Yang,[†] Aniruddha Joi,[‡] Yezdi Dordi,[‡] Nikhil Dole,[‡] and Stanko R. Brankovic^{*,†} 

[†]Cullen College of Engineering, University of Houston, Houston, Texas 77204, United States

[‡]Lam Research Corporation, Fremont, California 94538, United States

ABSTRACT: The present work demonstrates an electroless (e-less) deposition of Pb monolayer on Au and Cu surface whose morphology and properties resemble its underpotentially deposited counterpart. Our results and analysis show that the e-less Pb monolayer deposition is a surface selective, surface controlled, self-terminating process. Results also show that the electroless Pb monolayer deposition is enabling a phenomenon for new deposition method called “electroless atomic layer deposition” (e-less ALD). Here, the e-less Pb monolayer serves as reducing agent and sacrificial material in surface limited redox replacement reaction with noble metal ions such as Ptⁿ⁺, i.e., Pt deposition. The e-less ALD is highly selective to the metal substrates at which Pb forms the e-less monolayer. The full e-less ALD cycle leads to an overall deposition of a controlled amount of the noble metal. Repetition of the two-step e-less ALD cycle an arbitrary number of times leads to formation of a highly compact, smooth, and conformal noble metal thin film with applications spanning from catalyst synthesis to semiconductor technology. The process is designed for (but not limited to) aqueous solutions that can be easily scaled up to any size and shape of the substrate, deeming its wide applications.



1. INTRODUCTION

Improved understanding of nucleation kinetics of thin films has led to discoveries of new deposition protocols and concepts in which the thin film growth was manipulated to enhance the evolution of atomically flat epitaxial overlayers.^{1–3} Exploiting some of these results, new approaches were developed where the underpotentially deposited (UPD) monolayer is used to significantly improve the morphology of electrodeposited thin films.^{4–7} The latest example,⁷ so-called, “deposition via surface limited redox replacement (SLRR) of UPD monolayer,” has gained a lot of applications for synthesis of monolayer catalysts and noble metal thin films with different functionalities.^{8–15} The basic description of this deposition approach can be presented as combination of the potential controlled step (formation of UPD monolayer) and the electroless step representing the SLRR of UPD monolayer by more noble metal ions, i.e., galvanic displacement.⁷ The underlying phenomena controlling the morphology of the deposit and SLRR reaction kinetics have been studied and well understood.^{16–21} However, recent works show that there is still a lot of room for improvements and further simplifications of this deposition approach.^{22–24} These efforts point to the fact that better practicality, control, and cost effectiveness of the metal deposition via SLRR of UPD monolayer should enable expanded applications of this deposition approach into the areas of technology where traditional vacuum deposition methods are currently used.

In this paper we present results demonstrating an electroless (e-less) deposition of Pb monolayer (e-less Pb ML) whose morphology and properties resemble its UPD counterpart. The e-less Pb monolayer deposition is proved on Au and Cu substrates. Furthermore, we show that the e-less Pb monolayer deposition is enabling a phenomenon for new deposition method we call “electroless atomic layer deposition” (e-less ALD). Here, the e-less deposited Pb monolayer is used as reducing agent and sacrificial material in SLRR reaction with noble metal ions such as Ptⁿ⁺, i.e. Pt deposition. The results demonstrate that deposition process is highly selective to the metal substrates at which Pb forms the e-less ML. The full e-less ALD cycle involves sequential exposure of the substrate (Au and/or Cu) to the solution for electroless Pb monolayer deposition and then to the solution for SLRR reaction and noble metal deposition (Pt). This leads to an overall deposition of controlled amount of the noble metal in each cycle. Repetition of the two-step e-less ALD cycle an arbitrary number of times leads to formation of a highly compact, smooth, and conformal noble metal thin film with applications spanning from catalyst synthesis to semiconductor technology. The process is designed for (but not limited to) aqueous solutions that can be easily

Received: July 10, 2018

Revised: August 22, 2018

Published: September 4, 2018

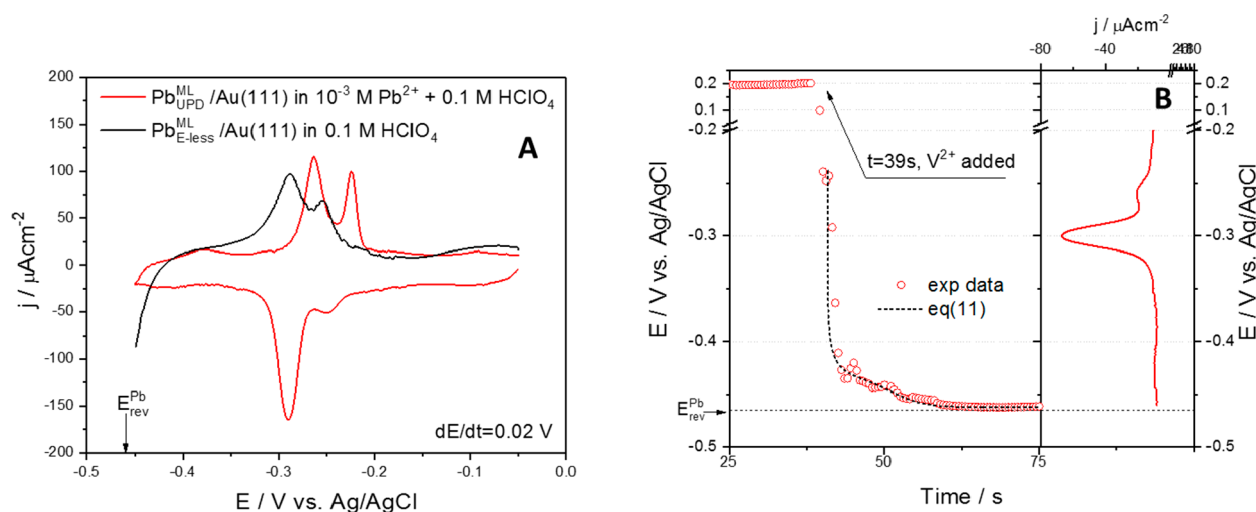


Figure 1. (A) Cyclic voltammetry of the Pb underpotential deposition/stripping process (red line) and linear sweep voltammetry of the e-less Pb monolayer stripping (black line) from Au(111) surface. (B) Open circuit transient during e-less Pb ML deposition (red dots) and Pb UPD monolayer deposition (red line) on Au(111) surface (cathodic sweep from (A)). The nominal concentration of Pb^{2+} in the solution during e-less Pb ML deposition is 0.67×10^{-3} M. Black dotted line represents eq 11 fit to the OCP data. The Pb reversible potential, $E_{\text{rev}}^{\text{Pb}}$, is indicated on both graphs.

scaled up to any size and shape of the substrate deeming its wide applications.

2. EXPERIMENTAL SECTION

2.1. General Details. The starting Au(111) was disk with diameter 10 mm and 3 mm thickness (Monocrystals Company). It was prepared using mechanical polishing, electropolishing, and hydrogen flame annealing. This routinely yielded a highly reflective mirrorlike surface with very reproducible Pb UPD voltammetry (Figure 1A). The Cu polycrystalline substrates were 100–200 nm thick films deposited on SiO_2/Si wafers which were reduced in $\text{H}_2 + \text{CO}$ gas mixture at 250°C for 1 h before the experiments. All solutions for Pb monolayer deposition and SLRR reaction were prepared with high purity grade chemicals such as PbO , VCl_2 , HClO_4 , and H_2PtCl_4 (99.999%, Alfa Aaesar, Merck) and >18.2 M Ω ultrapure water (Millipore Direct Q-UV with Barnstead A1007 predistillation unit). Before each experiment, solutions were deaerated for at least 1 h with ultrapure nitrogen in order to minimize the concentration of dissolved oxygen from air. All experiments were performed using ultraclean glassware and oxygen-free environment. The volume of the electrochemical cell was 0.150 dm^{-3} while the amount/volume of the reaction solution was standardized to 0.1 dm^{-3} for each experiment. The volume of the solution during electrochemical quartz microbalance (ECQMB) studies and during in situ scanning tunneling microscopy (STM) studies was 0.001 dm^3 . The quartz microbalance sample was a 50 nm thick gold film deposited on a 2 nm Cr seed on a quartz disk with a resonant frequency of $\approx 6 \text{ kHz}$. All potentials in the text are presented vs silver–silver chloride reference electrode ($\text{Ag}/\text{AgCl}/1.0 \text{ M KCl}$; $E = 0.235 \text{ V}$ vs SHE). The electrochemical studies were performed using a BAS Epsilon system, while ECQMB experiments were performed using a Metrohm Autolab PGSTAT 12 with integrated ECQMB module. The STM and atomic force microscopy (AFM) images were recorded using a Nanoscope V controller with a multimode scanner unit (Veeco instruments). The solution for e-less Pb ML deposition was prepared by mixing two volume part of the solution containing Pb^{2+} ions and one volume part of the solution containing V^{2+} ions. Both solutions contained 0.1 M HClO_4 as a background electrolyte. The nominal concentrations of Pb^{2+} and V^{2+} in solution for the e-less Pb ML deposition are presented in Table 1. Description of the solution for Pt deposition via SLRR of the e-less Pb ML is shown in Table 1 as well.

2.2. Experimental Routine. All deposition experiment and the open circuit potential (OCP) measurements during the e-less Pb ML deposition were performed in N_2 filled glovebox using either Au(111) or Cu polycrystalline films as substrates. In the case of Au crystal, the

Table 1. Solutions for the E-less Pb ML Deposition and for the Pt Deposition via SLRR of the E-less Pb ML

e-less Pb monolayer deposition	Pt deposition via SLRR of Pb monolayer
0.1 M HClO_4	0.1 M HClO_4
$10^{-3}/0.67 \times 10^{-3} \text{ M Pb}^{2+}$	$0.001 \text{ M PtCl}_4^{2-}$
$3 \times 10^{-3} \text{ M V}^{2+}$	$0.3 \times 10^{-3} \text{ M Cl}^-$

hanging meniscus electrode configuration was used. In the case of Cu films, the samples were simply immersed into the Pb^{2+} containing solution. The entire experiment involved three steps. They are briefly explained below:

Step one: First, the cyclic voltammetry measurements were performed to verify the quality of the surface and characteristics of the Pb UPD process on a given surface (Au or Cu).

Step two: The potential is switched to the open circuit and OCP transients are recorded during the addition of V^{2+} containing aliquot. Typical length of the OCP measurements was between 50 and 100 s.

Step three: The sample with deposited e-less Pb ML is transferred to a well deaerated 0.1 M HClO_4 solution and the linear sweep is performed in anodic direction to strip the Pb ML and record the stripping charge.

The same experimental routine is also performed during ECQMB measurements, except the third step was omitted. In the case of the multilayer growth of Pt on Cu thin films and microwires, the automated set up for e-less ALD was used which was custom-made in our lab. The sample resided on the spinning platform which was synchronized with 3 solutions dispensers on top of the sample and all of them were integrated into a computer controlled loop. During exposure of the sample to the e-less Pb ML deposition solution, rinsing solution (H_2O), or Pt SLRR solution, the sample was kept stagnant for a certain time to allow the deposition to occur. However, in between each solution exposure step in the single ALD cycle, the sample was spun at 400 rpm to remove either solution. This way, a completely automated deposition of up to 100 e-less ALD cycles was performed without any manual sample manipulation.

3. RESULTS AND DISCUSSION

3.1. Electroless Pb Monolayer Deposition on Au(111).

The cyclic voltammetry result for the Pb UPD ML deposition on Au(111) in $10^{-3} \text{ M Pb}^{2+} + 0.1 \text{ M HClO}_4$ solution is shown in Figure 1A (red line). The Pb UPD on Au(111) represents a

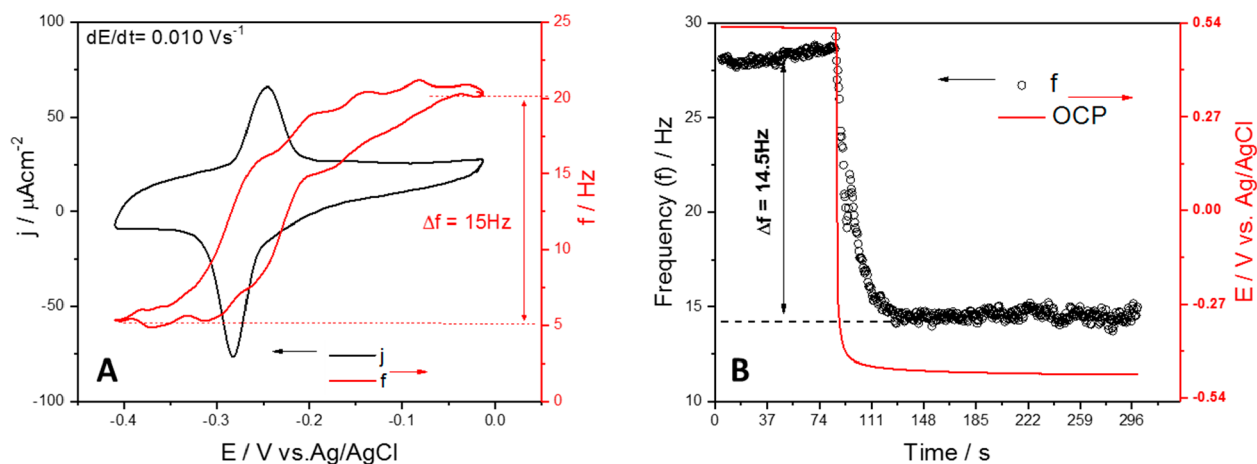


Figure 2. (A) Cyclic voltammogram (black line) and the corresponding change in resonant frequency of the quartz crystal (red line) during Pb underpotential deposition/stripping from Au surface (solution: 0.01 M Pb^{2+} + 0.1 M HClO_4). (B) Resonant frequency change of the quartz crystal (black dots) and the corresponding open circuit potential transient (red line) during e-less Pb ML deposition on Au surface (solution: 0.67×10^{-3} + 0.1 M HClO_4).

single phase system, and the complexity of the voltammogram is related to a different energetics of the adsorption sites on the Au surface.^{18,25} The shape of the deposition and stripping peaks and their corresponding potentials in Figure 1A are in agreement with literature data.²⁶ They are also indicative of very good quality of starting Au(111) surface. For the interest of further discussion, we note that the Pb UPD wave starts at approximately -0.2 V with a broad shoulder of a smaller peak related to a Pb deposition on terrace defects and steps. The main Pb UPD ML peak, centered at ≈ -0.28 V, corresponds to a Pb ML nucleation and densification on the terrace sites.²⁶ The Pb UPD ML stripping wave starts at ≈ -0.3 V. It is characterized by two peaks which correspond to the Pb UPD stripping from terrace sites (-0.255 V) and steps and surface defects (-0.225 V). Our measurements indicate that no Pb ML is present at the Au(111) for the potentials more positive than -0.2 V. After completed CV, the cell is switched to the open circuit, and the OCP of Au(111) gradually drifts to its steady state at $+0.2$ V, Figure 1B. The V^{2+} containing aliquot is added at $t = 39$ s, upon which the OCP of the Au(111) surface start to change abruptly toward more negative values. It reaches its steady state ($E_{\text{OCP}}^{\text{S}} = -0.46$ V) after ≈ 20 s. The value of $E_{\text{OCP}}^{\text{S}}$ is only a few millivolts more positive than the Pb reversible potential indicated in the graph with a dotted line. For comparison, on the right side of Figure 2B, the deposition wave from the UPD CV is plotted having a common potential axes. One can see that the value of the OCP drifts through the entire region of the Pb UPD ML formation and stability. The important results is that the value of $E_{\text{OCP}}^{\text{S}}$ resides in the potential region where the full Pb UPD ML is formed/stable during CV. This suggests that, in the solution with both, V^{2+} and Pb^{2+} ions, the Pb ML on Au(111) should be stable too. To verify this, and prove that actual deposition of Pb has happened, the Au crystal is immediately transferred into 0.1 M HClO_4 solution and linear sweep is performed in anodic direction with starting potential being the value of the OCP. The stripping wave for the e-less Pb is shown in Figure 1A, black line. It is evident that the qualitative shape of the e-less Pb stripping wave is very similar to the one corresponding to a stripping of a full Pb UPD ML. The stripping wave consists of two distinct peaks which are separated by $\Delta E = 0.03$ V. Importantly, the same potential difference between the two stripping peaks for the full Pb UPD ML is observed too. This indicates that stability

of the e-less Pb deposit is likely determined by the energetics of the surface adsorption sites which are in both cases the same (same Au surface). Therefore, we conclude that the ML of Pb is deposited as a result of the addition of V^{2+} aliquot in the Pb^{2+} containing solution. This statement is also supported by already discussed value of $E_{\text{OCP}}^{\text{S}}$ being in the potential range where a full Pb UPD ML is stable on Au(111). Therefore, we expect a 2D morphology for the e-less Pb ML as well. The measured stripping charge under the both curves in Figure 1A is almost the same, $q_{\text{e-less}}^{\text{S}} = 315 \pm 7 \mu\text{C}\cdot\text{cm}^{-2}$ and $q_{\text{UPD}}^{\text{S}} = 307.5 \pm 11 \mu\text{C}\cdot\text{cm}^{-2}$ and it is comparable to the results reported in the literature for the Pb UPD on Au(111).²⁵

These facts additionally strengthen the presumption that the e-less Pb deposition under conditions of our experiment results in a true 2D Pb ML formation. One interesting observation is that both stripping peaks related to the e-less Pb ML are shifted toward more negative values than the corresponding stripping peaks related to the Pb UPD ML. The difference is about 0.02 V. If we consider the fact that the stripping of e-less Pb ML is done in solution which does not contain any Pb^{2+} ions, then this observation is not surprising. We expect that the lack of Pb^{2+} ions in the solution shifts the Pb reversible potential toward more negative values and the Pb UPD stripping peak should be shifted accordingly expressing Nernstian behavior.^{27,28} In our case, the observed cathodic shift in stripping peaks of the e-less Pb ML does additionally proves its Pb UPD ML-like behavior.

To quantify the e-less Pb ML deposition process in more details and perform a comparative analysis with the Pb UPD, we performed ECQMB experiments following the same routine used to obtain the results in Figure 1. The CV of Pb UPD and corresponding frequency–potential dependence are shown in Figure 2A. The mass change on the Au/quartz electrode during a Pb UPD ML deposition/stripping corresponds to a resonant frequency change of 15 ± 1 Hz. The OCP and resonant frequency transients during the e-less Pb ML deposition are shown in Figure 2B. The resonant frequency change during the e-less Pb ML deposition is 14.5 ± 1 Hz. Obviously, both processes, the UPD of Pb ML and the e-less deposition of Pb ML produce almost an identical change in mass and the resonant frequency of the quartz crystal. Therefore, we conclude that the ECQMB and the charge stripping data are in full agreement, and

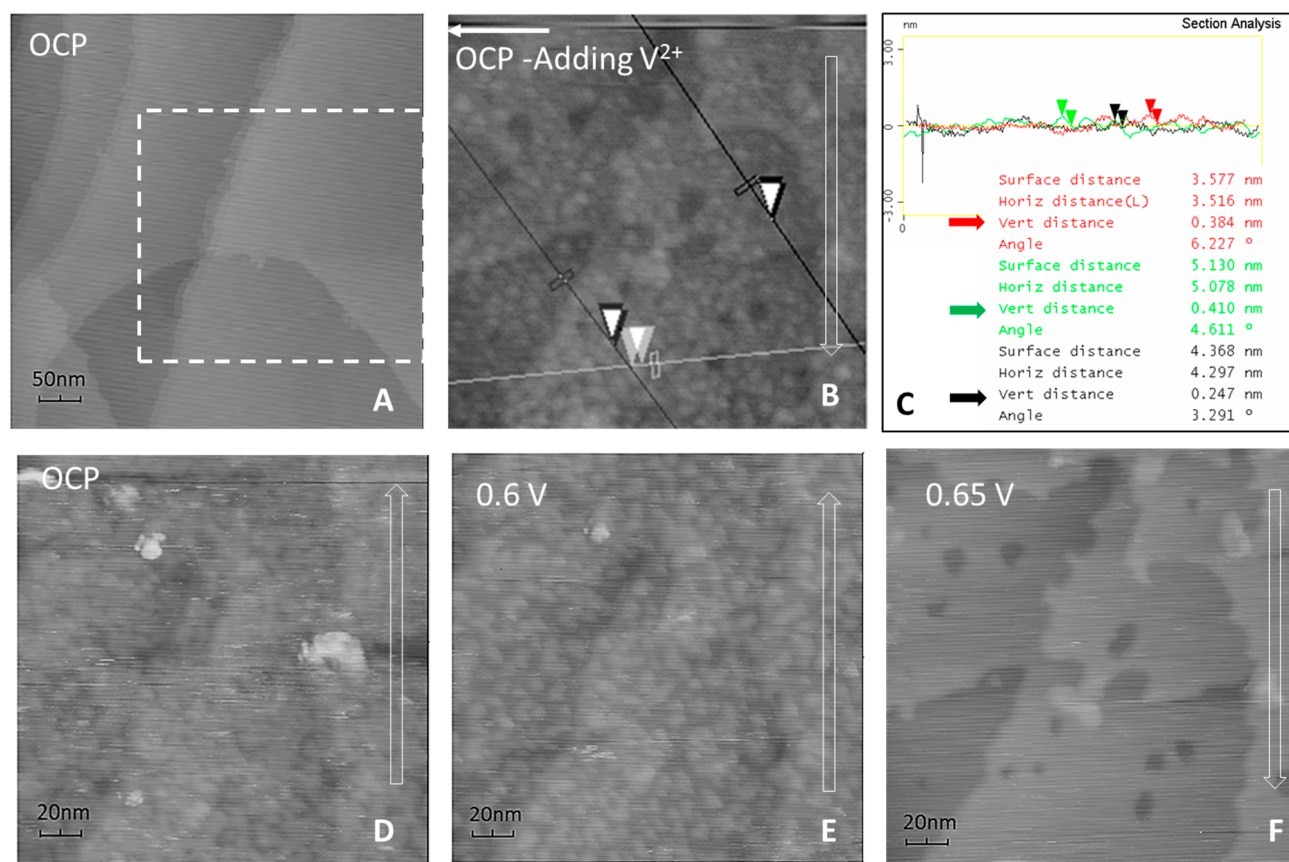


Figure 3. In situ STM images of the e-less Pb ML deposition/dissolution. Scan direction is indicated by the open arrow. Corresponding substrate potentials at which images are recorded are indicated in the upper left corner. STM image acquisition time is approximately 3 min. In image (B), the traces over which the cross-sectional measurements are taken are indicated by line/arrow combination. In image (C), the summary of the cross-sectional measurements and trace profile is presented.

that the e-less Pb ML has approximately the same atomic/mass areal density as the Pb UPD ML.

A more qualitative information about the e-less Pb ML deposition process and the e-less Pb ML morphological similarity with the Pb UPD ML were gained during our in situ STM investigation. The results are presented in Figure 3. Image (A) shows a clean Au(111) surface in solution with 10^{-3} Pb^{2+} + 0.1 M HClO_4 at open circuit (≈ 0.2 V). The characteristic features of a high quality single crystal Au surface can be recognized. The 200–300 nm wide terraces are separated by monatomic steps. The region of surface which was zoomed in for further study is indicated with a white quadrant. During the acquisition of image (B), the V^{2+} containing aliquot is added to the STM cell. The moment of addition is indicated in the image with an arrow. The Au surface was kept at OCP conditions. As the scan continued, the surface morphology shows roughening and nucleation of numerous 3 nm–5 nm size 2D clusters with atomic height between 0.25 and 0.41 nm. The cross-sectional measurements from the traces spanning over the three different positions (clusters) shown in image (B) are summarized in image (C) presented as a direct output from our STM analysis software. The height of the clusters fall in the range of the dimensions expected for a Pb or Au adatom. Therefore, a 2D nature of the nucleation process is confirmed. An important observation is that during acquisition of image B, the OCP drifts though the potential region where the e-less Pb ML forms as shown in Figure 1B (-0.2 V to -0.46 V). Therefore, the morphological changes on the Au surface observed by the STM

are associated with the onset and progression of the e-less Pb ML deposition. Further on, in image (D), one can see a gradual smoothing of the surface and merging of the 2D clusters into a continuous layer, i.e., a full monolayer. At the same time, the OCP of Au surface reaches its steady state, $E_{\text{OCP}}^S \approx -0.46$ V. It is apparent that the quality of the image (D) starts to deteriorate somewhere around the second half of the scan, and the noise level becomes significant. The reason for this is the low potential bias on the PtIr tip which was kept constant during imaging, $E_{\text{bias}}^{\text{tip}} = 0.03$ V. Because of that, the STM tip has also drifted into the potential range where the H^+ reduction proceed on the tip surface and Pb UPD ML on PtIr surface becomes stable. Consequently, each process resulted in worsening of the image quality. To mitigate this problem, the potential control is established and potentials more positive than the region of the e-less Pb UPD ML stability on Au surface were applied. This restored the imaging quality and we started to observe the e-less Pb ML dissolution. The results are shown in images (E) and (F).

Similar to the case of the Pb UPD ML stripping,²⁹ the STM images indicate that dissolution of the e-less Pb ML starts from the terrace sites and proceeds with gradual 2D Pb cluster dissolution. The clean Au surface is restored in image F at the potential of 0.65 V. One can see that the ending Au surface (image F) has a higher density of defects than the starting one shown in image A. This is the consequence of the surface alloying between the Pb ML and Au which was reported earlier in studies of the Pb UPD on Au.³⁰ It is important to notice that the applied potential producing the complete e-less Pb ML

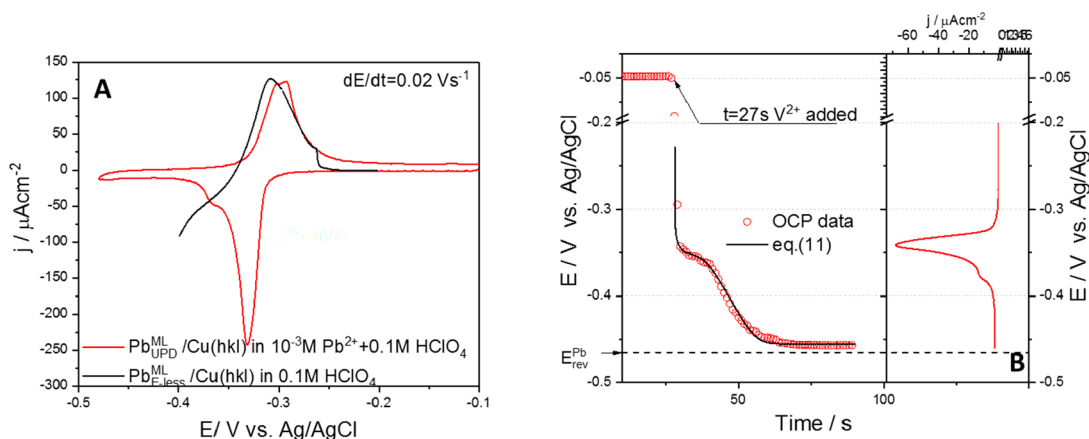


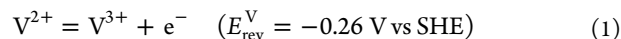
Figure 4. (A) Cyclic voltammetry of the Pb underpotential deposition/stripping process (red line) and linear sweep voltammetry of the e-less Pb monolayer stripping (black line) on/from the Cu(*hkl*) surface. (B) Open circuit transient during e-less Pb ML deposition (red dots) and Pb UPD monolayer deposition (red circles) on Cu(*hkl*). The nominal concentration of Pb²⁺ in the solution during e-less Pb ML deposition is 0.67×10^{-3} M. Black dotted line represents eq 11 fit to the OCP data. The Pb reversible potential, $E_{\text{rev}}^{\text{Pb}}$ is indicated in (B).

stripping in our insitu STM experiments had to be much more positive than one applied in our voltammetry experiment, Figure 1A. The reason for this is that the solution in STM cell still contained a significant amount of V²⁺ as a reducing agent. Thus, before the electrochemical stripping of e-less Pb ML can be observed, a large reducing power of remaining V²⁺ ions had to overcome which required application of a much more positive potential.³¹ The additional reason for seeing delayed dissolution of e-less Pb monolayer is perhaps the STM tip shielding which was known to slow down the electrochemical dissolution/deposition process.

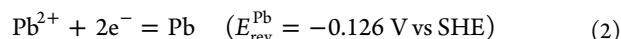
3.2. Electroless Pb ML Deposition on Cu(*hkl*). The characteristic cyclic voltammetry of Pb UPD on the Cu thin film sample (Cu(*hkl*)) is shown in Figure 4A (red line). The main feature of the CV is the deposition peak that starts at ≈ -0.3 V, centered at -0.335 V. The region of CV where the full Pb UPD ML is present on Cu(*hkl*) is between -0.4 V and Pb reversible potential. The Pb UPD ML stripping peak starts at ≈ -0.35 V, and it is centered at -0.3 V. Overall, the qualitative appearance of Pb UPD on our Cu(*hkl*) sample resembles to a great extent the Cu UPD on Cu(111) surface.³² Following the experimental routine previously described, after the full CV is recorded, the potential control is turned off, and the OCP transient is recorded during addition of V²⁺ containing aliquot. These data are presented in Figure 4B. As in the experiment with Au(111), with addition of V²⁺ ($t = 27$ s), the OCP starts to change abruptly and drifts toward more negative values. Approximately at $t = 75$ s, the OCP transient enters a steady state with $E_{\text{OCP}}^{\text{S}} \approx -0.455$ V. Similar to the experiment with Au(111), the value of $E_{\text{OCP}}^{\text{S}}$ is only few millivolts more positive than the reversible potential of Pb indicated by dotted line in Figure 4B. Comparing the OCP data with the deposition wave from the CV of the Pb UPD on Cu(*hkl*), in Figure 4B, an important result becomes evident. The complex shape of the OCP transient resembling a staircase starts to develop at approximately same potential where the main Pb UPD peak occurs. This type of correlation between the OCP for e-less Pb ML deposition and the Pb UPD ML deposition potential was not observed on Au(111) surface. However, this was very reproducible behavior in all our e-less Pb ML deposition experiments on Cu(*hkl*). Therefore, we consider it as an indicator of the e-less Pb ML formation on our Cu(*hkl*) surface. Similar to our experiments with Au(111), for the Cu(*hkl*) surface, we found very good agreement between the

stripping charge of the e-less Pb ML ($290 \pm 22 \mu\text{C}\cdot\text{cm}^{-2}$, black line in Figure 4A) and stripping charge of the Pb UPD ML ($280 \pm 15 \mu\text{C}\cdot\text{cm}^{-2}$, red line, Figure 4A). The stripping charges are somewhat lower than the literature data for the Pb UPD on Cu(111) surface.³² The reason for this is that the Cu thin films were subjected to CMP process upon the deposition in order to obtain ultimately smooth layers. Perhaps some Cu surface contamination due to CMP chemistry could contribute to the observed charge discrepancy. Other reason could be an incomplete Cu-oxide reduction during annealing stage. However, we conclude that the addition of V²⁺ into Pb²⁺ containing solution under described conditions leads to formation of the Pb ML on Cu(*hkl*) surface.

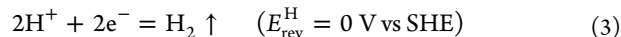
3.3. Analytical Model and OCP analysis. In our e-less Pb ML deposition experiments, we do recognize that the V²⁺ ion is the reduction agent, i.e., the electron producing reaction is the oxidation of the V²⁺ ion to V³⁺:



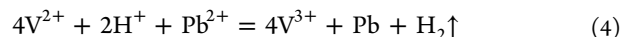
On the other hand, the electron consuming reaction is the Pb²⁺ ion reduction, i.e., Pb deposition:



The parasitic electron consuming reaction which has to be taken into account is the proton (H⁺) reduction, i.e., the hydrogen evolution reaction:



For the sake of simplifying our modeling effort we neglect the oxygen reduction as the additional electron consuming reaction which occurs in parallel with the reactions 2 and 3. The reason for this is that all solutions in our experiments were well deaerated and dissolved oxygen routinely reached levels below 5×10^{-6} M. This is much lower than the concentration of H⁺ (1 M, pH = 1) which makes the proton reduction a dominant “parasitic” reaction. Therefore, combining eqs 1–3, the full redox process involved in the e-less Pb ML deposition is presented as



The attempts to analyze the OCP data during the e-less Pb ML deposition using the standard mix-potential theory

approach did not yield any meaningful outcome.³³ The reason is that $E_{\text{OCP}}^{\text{S}}$ values in each experiment were more positive than the Pb reversible potential ($E_{\text{OCP}}^{\text{S}} > E_{\text{rev}}^{\text{Pb}}$) which mixed potential theory fails to predict. Furthermore, the Pb deposition was limited to a ML, while the expected outcome from mixed potential analysis was to predict Pb bulk deposition in the overpotential region. Because of that, we resume the effort to develop a different model to analyze the OCP data. Developing our model, we have made some assumption based on the realistic description of the e-less deposition systems and solutions. We assumed that all reactions (eqs 1–3) involved in the e-less Pb ML deposition process are kinetically limited and that transport limitations are not reached at any point during experiments. The rationale for this is relatively high concentration and large total amount of V^{2+} in the reaction solution and slow kinetics of H^+ reduction on Au, Cu and Pb surfaces.^{34,35} In addition to this, we also realize that the e-less Pb deposition is limited to a monolayer, and for a given Pb^{2+} concentration it cannot lead to any depletion of the Pb^{2+} ions at the interface. Furthermore, we do consider that our surface is the catalyst for oxidation and reduction reactions discussed previously, and therefore, we distinguish possibility of having different kinetics and reaction rates for V^{2+} oxidation and H^+ reduction on the clean substrate (Cu(*hkl*) and Au(111)) surface ($R_V^{\text{S}}, R_H^{\text{S}}$) and on the substrate surface covered by Pb adatoms (R_V^{ML} and R_H^{ML}),

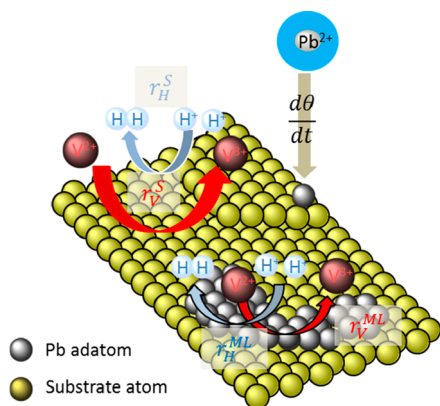


Figure 5. Schematic of the redox processes occurring on the clean substrate and Pb-covered substrate surface.

Hence, we can write a differential form of the rate equation for redox process described in eq 4 as follows:

$$\Gamma_{\text{ML}}^{\text{Pb}} \frac{d\theta}{dt} + (1 - \theta)R_{\text{H}}^{\text{S}} + \theta R_{\text{H}}^{\text{ML}} = (1 - \theta)R_{\text{V}}^{\text{S}} + \theta R_{\text{V}}^{\text{ML}} \quad (5)$$

The first term on the left side represents the rate of the Pb ML deposition described by eq 1 in $[\text{mol cm}^{-2} \text{ s}^{-1}]$ units. It is a product of the surface concentration of a full Pb ML on either the Au(111) or Cu(*hkl*) surface ($\Gamma_{\text{ML}}^{\text{Pb}}$, in $[\text{mol cm}^{-2}]$ unit) and the rate of Pb ML coverage increase ($\frac{d\theta}{dt}$, in $[\text{s}^{-1}]$ unit). The $(1 - \theta)$ and θ terms are introduced to describe the spatial partition between different reaction rates for hydrogen evolution (eq 3) and V^{2+} oxidation (eq 1) occurring on qualitatively different surfaces/catalysts, Figure 5. All rate terms in eq 5 also have $[\text{mol cm}^{-2} \text{ s}^{-1}]$ units. After performing a basic algebra and consolidation of the notation such that $r_{\text{H}}^{\text{S}} = R_{\text{H}}^{\text{S}}/\Gamma_{\text{ML}}^{\text{Pb}}$, $r_{\text{H}}^{\text{ML}} = R_{\text{H}}^{\text{ML}}/\Gamma_{\text{ML}}^{\text{Pb}}$, $r_{\text{V}}^{\text{S}} = R_{\text{V}}^{\text{S}}/\Gamma_{\text{ML}}^{\text{Pb}}$, and $r_{\text{V}}^{\text{ML}} = R_{\text{V}}^{\text{ML}}/\Gamma_{\text{ML}}^{\text{Pb}}$ one gets

$$\frac{d\theta}{(1 - \theta)(r_{\text{V}}^{\text{S}} - r_{\text{H}}^{\text{S}}) + \theta(r_{\text{V}}^{\text{ML}} - r_{\text{H}}^{\text{ML}})} = dt \quad (6)$$

In the above expression, all rates now have $[\text{s}^{-1}]$ units. The terms in the brackets represent the difference between the V^{2+} oxidation rate and hydrogen evolution (proton reduction) rate on the clean substrate (Au(111) or Cu(*hkl*)), ($r_{\text{V}}^{\text{S}} - r_{\text{H}}^{\text{S}}$) and substrate surface covered by the Pb adatoms, ($r_{\text{V}}^{\text{ML}} - r_{\text{H}}^{\text{ML}}$). They can be replaced by new notation such that $\Delta r_{\text{S}} = r_{\text{V}}^{\text{S}} - r_{\text{H}}^{\text{S}}$ and $\Delta r_{\text{ML}} = r_{\text{V}}^{\text{ML}} - r_{\text{H}}^{\text{ML}}$. Therefore, the eq 6 further consolidates to

$$\frac{d\theta}{\Delta r_{\text{S}} + \theta(\Delta r_{\text{ML}} - \Delta r_{\text{S}})} = dt \quad (7)$$

The above equation can be easily integrated as

$$(\Delta r_{\text{ML}} - \Delta r_{\text{S}}) \ln|\Delta r_{\text{S}} + \theta(\Delta r_{\text{ML}} - \Delta r_{\text{S}})| = t + C \quad (8)$$

The integration constant C is evaluated from the initial conditions; $t = 0$, $\theta = 0$, which yields $C = (\Delta r_{\text{ML}} - \Delta r_{\text{S}}) \ln|\Delta r_{\text{S}}|$. After substitution back in to eq 9 and rearrangement, the explicit θ vs t functional is obtained representing the integral form of the rate equation for the redox processes involved in the e-less Pb ML deposition:

$$\theta = \frac{\Delta r_{\text{S}}}{(\Delta r_{\text{ML}} - \Delta r_{\text{S}})} \left(\exp\left(\frac{t}{\Delta r_{\text{ML}} - \Delta r_{\text{S}}}\right) - 1 \right) \quad (9)$$

At $t \rightarrow 0$ limit, the mathematical form of eq 9 accurately predicts the value of $\theta = 0$. However, in order to have a true physical meaning at $t \rightarrow \infty$ limit, certain mathematical relations between Δr_{ML} and Δr_{S} have to be satisfied. The first one is that the sign of the exponential term has to be negative in order to have the exponential function with asymptotic decay. This enforces condition for $\Delta r_{\text{ML}} - \Delta r_{\text{S}}$ to be < 0 . The second relation is that the ratio $\Delta r_{\text{S}}/(\Delta r_{\text{ML}} - \Delta r_{\text{S}})$ must be also negative. Both relations combined yield the functional (eq 10) with positive asymptote $\theta = -\Delta r_{\text{S}}/(\Delta r_{\text{ML}} - \Delta r_{\text{S}})$, for $t \rightarrow \infty$ limit. This is realistic prediction which suggests that the coverage of the e-less Pb ML reaches its maximum after certain time, i.e., after the time necessary for OCP transient to reach its steady state, $E_{\text{OCP}}^{\text{S}}$. A closer examination of the two relations imposed by the physical validity of the rate equation model also yields an additional implication about the sign of Δr_{ML} and Δr_{S} terms. Both terms have to be positive; $\Delta r_{\text{ML}}, \Delta r_{\text{S}} > 0$. This result is expected. It suggests that the e-less Pb ML deposition occurs (eq 2) on either part of the surface only if the V^{2+} oxidation (eq 1) produces more electrons than what is consumed by the parasitic hydrogen evolution (proton reduction) reaction (eq 3). Therefore, $\Delta r_{\text{S}} = r_{\text{V}}^{\text{S}} - r_{\text{H}}^{\text{S}} > 0$ and $\Delta r_{\text{ML}} = r_{\text{V}}^{\text{ML}} - r_{\text{H}}^{\text{ML}} > 0$ is required from physical validity of the model and the stoichiometry of the e-less Pb ML deposition, eq 4. However, the $\Delta r_{\text{ML}} - \Delta r_{\text{S}} < 0$ relation together with $\Delta r_{\text{ML}}, \Delta r_{\text{Au}} > 0$ condition also implicates that $\Delta r_{\text{S}} > \Delta r_{\text{ML}}$. This is an important result that has to be looked in more detail. It suggests that, in order for the e-less Pb ML deposition to occur, the catalytic properties of the clean substrate and Pb adatom-covered substrate surface have to be quite different when considering mutual rates of V^{2+} oxidation and H^+ reduction reactions. The e-less Pb ML deposition will proceed only if the difference in V^{2+} oxidation and H^+ reduction rates are larger for the clean substrate surface than for the surface covered by Pb adatoms. This modeling result also suggest that Pb ML deposition proceeds only if there is available free substrate surface.

Table 2. Parameters Related to the Details of E-less Pb ML Deposition Obtained from the eq 11 Fit to OCP Data in Figures 1B and 4B^a

surface	$E_{\theta \rightarrow 0}$ [V]	parameters of the fit		calcd values	
		$\frac{\Delta r_s}{(\Delta r_{ML} - \Delta r_s)}$	$\Delta r_{ML} - \Delta r_s$, [s ⁻¹]	Δr_s , [s ⁻¹]	Δr_{ML} , [s ⁻¹]
Au(111)	-0.21 ± 0.015	-0.996 ± 0.001	-2.38 ± 0.004	2.37 (Δr_{Au})	0.01
Cu(<i>hkl</i>)	-0.274 ± 0.008	-0.9999993 ± 10 ⁻⁷	-2.17 ± 0.02	2.16591 (Δr_{Cu})	4.09 × 10 ⁻³

^aThe value of the RT/mF term is taken as 0.0129 V assuming $m = 2$ and $T = 300$ K.

In order to have a complete E vs t model to interpret our OCP data during the e-less Pb ML deposition, we assume that the thermodynamic stability, i.e., adsorption isotherm for the e-less Pb ML on Au or Cu is qualitatively the same as for its UPD Pb ML counterpart. This assumption is based on the results presented in Figures 1A and 4A where the qualitative shape of the e-less Pb ML stripping peaks is the same as that for the stripping of the Pb UPD ML. In addition, the STM data presented in Figure 3 do indicate that deposition and dissolution of the e-less Pb ML on Au(111) occurs in the same manner as what has been reported for Pb UPD ML.²⁹ Therefore, we proceed by using the one of the UPD adsorption isotherm models reported in the literature to interpret the e-less Pb ML coverage vs potential (OCP) behavior. We choose the general adsorption isotherm developed by Swathirajan and Bruckenstein (S-B isotherm in further text) which applies to virtually any UPD system.³⁶ In our derivations, we limit our attention to the form of the isotherm representing the single phase UPD systems where the electroadsorption valence of the UPD adatoms is equal to the oxidation state of the metal ions.¹⁹ In this case, the S-B isotherm has the form:

$$E = E_{\theta \rightarrow 0} - \frac{RT}{mF} \ln \left\{ \left(\frac{\theta}{1 - \theta} \right) + f\theta + g\theta^{3/2} \right\} \quad (10)$$

The $E_{\theta \rightarrow 0}$ term represents the potential where the UPD ML approaches zero coverage. The f term is *Temkin* parameter describing the UPD adatom–substrate interactions. The g term is the *Frumkin* parameter describing the interactions among the UPD adatoms within the UPD ML. Combining the adsorption isotherm model, eq 10, with the rate equation model, eq 9, yields the final form of the E vs t functional that is used to analyze our OCP transients during the e-less Pb ML deposition process;

$$E = E_{\theta \rightarrow 0} - \frac{RT}{mF} \times \ln \left\{ \left(\frac{(\Delta r_s / (\Delta r_{ML} - \Delta r_s)) (\exp(t / (\Delta r_{ML} - \Delta r_s)) - 1)}{1 - (\Delta r_s / (\Delta r_{ML} - \Delta r_s)) (\exp(t / (\Delta r_{ML} - \Delta r_s)) - 1)} \right) + f(\Delta r_s / (\Delta r_{ML} - \Delta r_s)) (\exp(t / (\Delta r_{ML} - \Delta r_s)) - 1) + g((\Delta r_s / (\Delta r_{ML} - \Delta r_s)) (\exp(t / (\Delta r_{ML} - \Delta r_s)) - 1))^{3/2} \right\} \quad (11)$$

The results from fitting eq 11 to the OCP transients (dark dashed line) in Figures 1B and 4B are presented in Table 2.

As one can see, the eq 11 succeeds to capture all features of the OCP transients presented in Figures 1B and 4B. Indeed, the quality of the fit in each case yielded r^2 values better than 0.97. Importantly, the extracted parameters of the fit, presented in the Table 2, all have realistic values and therefore a true physical meaning. This allows us to address the mechanism of the e-less Pb ML deposition in more detail. First, we recognize that the value of $E_{\theta \rightarrow 0}$ for each surface falls in the potential region more

positive than the corresponding Pb UPD peak which is in agreement with the physical description of this parameter. Furthermore, the values of the $\Delta r_s / (\Delta r_{ML} - \Delta r_s)$ and $(\Delta r_{ML} - \Delta r_s)$ are <0 which was postulated by the physical validity of the model. For both surfaces, the absolute values of $\Delta r_s / (\Delta r_{ML} - \Delta r_s)$ are very close to 1, which means that the coverage of the e-less Pb ML is ≈ 1 . Therefore, the model fit to the OCP data yields parameters whose values and interpretation are in very good agreement with physical picture of the e-less Pb ML deposition process derived from our experiments; stripping measurements, ECQMB and STM results (Figures 1–4). From parameters of the fit, we can calculate values of Δr_{ML} and Δr_s . They are >0 and, more importantly, the $\Delta r_s \gg \Delta r_{ML}$ as postulated by the model, eq 9. It is important to notice that values of Δr_{ML} for both surfaces are practically zero. From the redox kinetics point of view, this means that no net electrons for Pb²⁺ reduction are produced on the substrate surface covered by the Pb adlayer. Therefore, Pb deposition occurs only if there is available clean substrate, i.e., $(1 - \theta) > 0$. This result can be understood as a consequence of the lacking catalytic potential of Pb adlayer to support V²⁺ oxidation (eq 1). This leads to $r_V^{ML} \approx 0$, $\Rightarrow \Delta r_{ML} \approx 0$ as a plausible scenario. We can derive this conclusion from several facts related to the adsorption of V²⁺ ion ($\{V(H_2O)_6\}^{2+}$) which is a prelude for its surface catalyzed oxidation. Earlier studies show that the difference in the electronegativity and electron affinity between metal consisting the UPD adlayer and substrates leads to the situation where the UPD adlayer surface is electron deficient, i.e., the UPD adatoms represent a positive side of the UPD adatom–substrate dipole.^{37,38} The same is expected in the case of the e-less Pb ML deposit and the Pb-covered Au or Cu surface as realistic scenario. For ion such as V²⁺, the electronic structure ($[Ar] 3d^3 4s^0$) requires that the adsorption bond with the metal surface is formed by electron donation from the surface atoms into an unoccupied 4s- and 3d-orbitals.³⁹ However, a positive charge on the Pb side of the Pb-substrate dipole does not create such conditions. Thus, the V²⁺ adsorption is unlikely to occur implicating $r_V^{ML} \approx 0$. In the case of the Cu or Au surface free from Pb adatoms, the adsorption of V²⁺ is enabled by Cu and Au metals' rich d-electron configuration ($[Ar] 3d^9 4s^2$ and $[Xe] 4f^{14} 5d^9 6s^2$) and their electron donation to unoccupied 3d-orbitals of the V²⁺ ion.⁴⁰ Therefore, $r_V^S > 0$, $\Rightarrow \Delta r_s > 0$ is expected. As a conclusion, we recognize that V²⁺ oxidation reaction occurring only on the parts of Au and Cu surface free from Pb adatoms which leads to the situation where the e-less Pb ML deposition is surface controlled, self-limiting process.

For the purpose of further analysis of the OCP data, it is useful to rewrite eq 5 to express the net deposition rate of Pb, $\frac{d\theta}{dt}$, as a function of the Δr_{ML} and Δr_s terms as

$$\frac{d\theta}{dt} = \theta \Delta r_{ML} + (1 - \theta) \Delta r_s \quad (12)$$

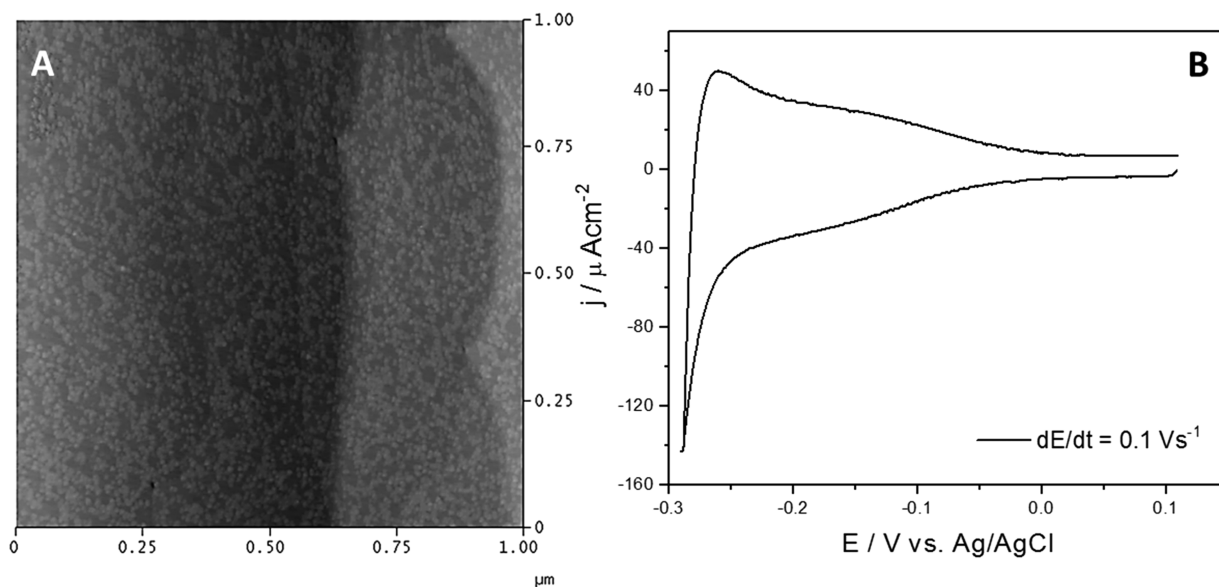


Figure 6. (A) STM image of Au(111) surface with Pt deposit after two e-less ALD cycles. (B) Cyclic voltammogram of the surface shown in (A) in 0.1 M HClO₄ (first cycle).

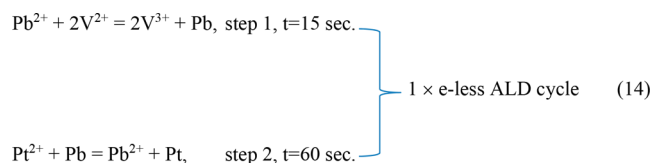
Considering that data in Table 2 suggests $\Delta r_{\text{ML}} \approx 0$, after accommodating this condition and substitution of eq 9 back to eq 12, one gets the description of the Pb ML deposition rate as

$$\frac{d\theta}{dt} \approx \exp\left(-\frac{t}{\Delta r_s}\right) \quad (13)$$

A slightly higher value of Δr_s for Au(111) than for Cu(*hkl*) ($\Delta r_{\text{Au}} > \Delta r_{\text{Cu}}$) indicates that the e-less Pb ML deposition rate is larger (deposition is faster) on the Au(111) than on the Cu(*hkl*) surface at any time ($t > 0$), Table 2. This observation brings few important points for discussion related to the catalytic nature of the substrate and its role in the e-less Pb ML deposition process. As discussed previously, the V^{2+} ion has to adsorb on the substrate surface in order for its oxidation to proceed (eq 1). At the same time, for any pathway of the hydrogen evolution reaction, the H^+ and H_{ads} intermediates have to be present at the surface as well.⁴⁰ Therefore, we expect that surface active sites are in competition for both; V^{2+} and H^+/H adsorption. Earlier works showed that overpotential for hydrogen evolution on Cu surface is higher than that on Au which also correlates with the relative strength of the Cu–H and Au–H bonds but it has an opposite correlation with the rate of hydrogen evolution reaction, $r_{\text{H}}^{\text{Au}} > r_{\text{H}}^{\text{Cu}}$.⁴¹ Within the realm of our discussion, we expect that comparatively stronger bond of H_{ads} to the Cu surface results in the larger portion of the active sites covered with H_{ads} on Cu as compared to Au surface. Hence, we expect that V^{2+} will have less chances to adsorb on the active site on the Cu than on the Au surface. This leads to comparatively slower kinetics for V^{2+} oxidation on Cu surface than on Au surface, i.e., $r_{\text{V}}^{\text{Au}} > r_{\text{V}}^{\text{Cu}}$. Hence, we contemplate that the substrate exhibiting a faster hydrogen evolution (proton reduction) kinetics and lower energy for the hydrogen adsorption bond also provides a faster rate of the e-less Pb ML deposition ($\Delta r_{\text{Au}} > \Delta r_{\text{Cu}}$).

3.4. Electroless Atomic Layer Deposition. Discussed e-less Pb ML deposition is a new phenomenon which present an opportunity to further advance the deposition approaches based on SLRR. We demonstrate this by showing an example of Pt deposition via SLRR of the e-less Pb ML for Cu(*hkl*) and Au(111) substrates. The new deposition approach includes two

steps which are part of a full deposition cycle. Each step represents an e-less deposition process which is the part of the sequence consisting of successive substrate immersion/exposure to the solution for the e-less Pb ML deposition (step 1) and then to the solution for SLRR reaction (step 2, Pt deposition). The duration of each step in the ALD cycle is determined by examining the OCP transients (Figures 1 and 4) for e-less Pb ML deposition on Au or Cu (step 1) and our previous results studying the kinetics of Pt deposition via SLRR of Pb UPD ML¹⁸ (step 2). The described sequence mimics to a great extent the standard ALD cycle where the adsorption of the metal precursors and surface catalyzed reaction are replaced by the e-less Pb ML deposition and SLRR reaction. Because of that, we named the new deposition approach as “e-less atomic layer deposition” (e-less ALD), eq 14.



The first example of the e-less ALD is shown in Figure 6A. It represents the Pt deposit on Au(111) obtained by executing only two e-less ALD cycles. The STM image analysis shows that Pt coverage of the Au(111) is $\approx 70 \pm 5\%$ and that the overall Pt morphology is predominantly 2D consisting of the Pt nanoclusters which are partially merged into a larger agglomerates. Furthermore, the image analysis also shows that $\approx 21\%$ of Pt nanoclusters are two monolayers high which suggests that the overall amount of Pt deposited by the two e-less ALD cycles is ≤ 1 monolayer. This is close to what is expected by stoichiometry of SLRR reaction (1.3 ML) assuming that the e-less Pb UPD ML has the same areal density as Pb UPD ML and that the efficiency is 100%.

The electrochemical characterization of Pt/Au(111) deposit using cyclic voltammetry in 0.1 M HClO₄ is shown in Figure 6B. The results show that the Pt deposit exhibits the electrochemical activity characteristic for the Pt-bulk electrode demonstrated by ≈ 0.2 V wide region of hydrogen UPD, Figure 6B. Hence, the e-

SiO₂ fields. This is important results demonstrating an inherent surface selectivity of the e-less ALD process only to the substrates where the e-less Pb ML deposition phenomenon occurs. This result demonstrates also that surface selectivity of the e-less ALD process could provide a certain benefits when its integration is considered into a complex fabrication routes or substrate structures commonly seen in microelectronics, magnetic disk-drive, or MEMS technologies.

4. CONCLUSION

The experimental results, modeling, and data analysis demonstrate the new phenomenon of the electroless deposition of Pb ML on Au(111) and Cu(*hkl*) whose morphology and properties resemble those of its UPD counterpart. The e-less Pb ML deposition, in its nature, represents a surface selective, surface controlled, self-terminating process. These attributes are consequence of the synergy between particular properties of the redox processes and substrates involved in the e-less Pb ML deposition. The e-less Pb ML deposition is demonstrated to be an enabling phenomenon for development of the two-step e-less ALD cycle where the e-less Pb ML serves as a reducing agent in the SLRR reaction with noble metal ions, i.e., noble metal deposition. The full e-less ALD cycle results in an overall deposition of the controlled amount of noble metal which is the function of the areal density of deposited Pb ML and the stoichiometry of the SLRR reaction. The e-less ALD is highly selective to the metal substrates at which Pb forms an e-less ML, providing an advantage when certain manufacturing and integration requirements are considered. Repetition of the two-step e-less ALD cycle an arbitrary number of times leads to formation of a highly compact, smooth, and conformal noble metal thin films with applications spanning from catalyst synthesis to semiconductor technology.

AUTHOR INFORMATION

Corresponding Author

*E-mail: SRBrankovic@uh.edu.

ORCID

Stanko R. Brankovic: 0000-0001-8250-8382

Notes

The authors declare no competing financial interest.

ACKNOWLEDGMENTS

The experimental material is based upon work supported in part by the National Science Foundation under Contract CBET 1605331 and Lam Research Corporation gift grant.

REFERENCES

- (1) Zhang, Z.; Lagally, M. G. Atomistic Processes in the Early Stages of Thin-Film Growth. *Science* **1997**, *276*, 377.
- (2) Rosenfeld, G.; Servaty, R.; Teichert, C.; Poelsema, B.; Comsa, G. Layer-by-layer Growth of Ag on Ag(111) Induced by Enhanced Nucleation: A model Study for Surfactant-Mediated Growth. *Phys. Rev. Lett.* **1993**, *71*, 895.
- (3) Camarero, J.; Ferron, J.; Cros, V.; Gomez, L.; Vazquez de Parga, A. L.; Gallego, J. M.; Prieto, J. E.; De Miguel, J. J.; Miranda, R. Atomistic Mechanism of Surfactant-Assisted Epitaxial Growth. *Phys. Rev. Lett.* **1998**, *81*, 850.
- (4) Sieradzki, K.; Brankovic, S. R.; Dimitrov, N. Electrochemical Defect-Mediated Thin-Film Growth. *Science* **1999**, *284*, 138.
- (5) Brankovic, S. R.; Dimitrov, N.; Sieradzki, K. Surfactant Mediated Growth of Ag on Au(111). *Electrochem. Solid-State Lett.* **1999**, *2*, 443.

- (6) Hwang, S.; Oh, I.; Kwak, J. Electrodeposition of Epitaxial Cu (111) Thin Films on Au (111) Using Defect-Mediated Growth. *J. Am. Chem. Soc.* **2001**, *123*, 7176.
- (7) Brankovic, S. R.; Wang, J. X.; Adzic, R. R. Metal Monolayer Deposition by Replacement of Metal Adlayers on Electrode Surfaces. *Surf. Sci.* **2001**, *474*, L173.
- (8) Sasaki, K.; Wang, J. X.; Naohara, H.; Marinkovic, N.; More, K.; Inada, H.; Adzic, R. R. Recent Advances in Platinum Monolayer Electrocatalysts for Oxygen Reduction Reaction: Scale-up Synthesis, Structure and Activity of Pt Shells on Pd Cores. *Electrochim. Acta* **2010**, *55*, 2645.
- (9) Zhang, J.; Sasaki, K.; Sutter, E.; Adzic, R. R. Stabilization Platinum Oxygen-Reduction Electrocatalysts Using Gold Clusters. *Science* **2007**, *315*, 220.
- (10) Vasilic, R.; Dimitrov, N. Epitaxial Growth by Monolayer-Restricted Galvanic Displacement. *Electrochem. Solid-State Lett.* **2005**, *8*, C173.
- (11) Kim, Y.-G.; Kim, J. Y.; Vairavapandian, D.; Stickney, J. L. Platinum Nanofilm Formation by EC-ALE Via Redox Replacement of UPD Copper: Studies Using in-situ Scanning Tunneling Microscopy. *J. Phys. Chem. B* **2006**, *110*, 17998.
- (12) Vasilic, R.; Viyannalage, L. T.; Dimitrov, N. Epitaxial Growth of Ag on Au (111) by Galvanic Displacement of Pb and Tl Monolayers. *J. Electrochem. Soc.* **2006**, *153*, C648.
- (13) Viyannalage, L. T.; Vasilic, R.; Dimitrov, N. Epitaxial Growth of Cu on Au(111) and Ag(111) by Surface Limited Redox Replacement: An Electrochemical and STM Study. *J. Phys. Chem. C* **2007**, *111*, 4036.
- (14) Kim, J. Y.; Kim, Y.-G.; Stickney, J. L. Copper Nanofilm Formation by Electrochemical Atomic Layer Deposition: Ultrahigh-Vacuum Electrochemical and In Situ STM Studies. *J. Electrochem. Soc.* **2007**, *154*, D260.
- (15) Venkatraman, K.; Dordi, Y.; Akolkar, R. Electrochemical Atomic Layer Deposition of Cobalt Enabled by the Surface Limited Redox Replacement of Underpotentially Deposited Zinc. *J. Electrochem. Soc.* **2017**, *164*, D104.
- (16) Gokcen, D.; Yuan, Q.; Brankovic, S. R. Nucleation of Pt Monolayers Deposited via Surface Limited Redox Replacement Reaction. *J. Electrochem. Soc.* **2014**, *161*, D3051.
- (17) Dimitrov, N. Recent Advances in the Growth of Metals, Alloys and Multilayers by Surface Limited Redox Replacement (SLRR) Based Approaches. *Electrochim. Acta* **2016**, *209*, 599.
- (18) Gokcen, D.; Bae, S.-E.; Brankovic, S. R. Reaction Kinetics of Metal Deposition Via Surface Limited Redox Replacement of Underpotentially Deposited Metal Monolayers. *Electrochim. Acta* **2011**, *56*, 5545.
- (19) Gokcen, D.; Bae, S.-E.; Brankovic, S. R. Stoichiometry of Pt Submonolayer Deposition via Surface-Limited Redox Replacement Reaction. *J. Electrochem. Soc.* **2010**, *157*, 582.
- (20) Bulut, E.; Wu, D.; Dole, N.; Kilic, H.; Brankovic, S. R. Reaction Kinetics of Metal Deposition via Surface Limited Redox Replacement of Underpotentially Deposited Monolayer Studied by Surface Reflectivity and Open Circuit Potential Measurements. *J. Electrochem. Soc.* **2017**, *164*, D159.
- (21) Dimitrov, N.; Vasilic, R.; Vasiljevic, N. A Kinetic Model for Redox Replacement of UPD Layers. *Electrochem. Solid-State Lett.* **2007**, *10*, D79.
- (22) Nutariya, J.; Fayette, M.; Dimitrov, N.; Vasiljevic, N. Growth of Pt by Surface Limited Redox Replacement of Underpotentially Deposited Hydrogen. *Electrochim. Acta* **2013**, *112*, 813.
- (23) Ambrozik, S.; Rawlings, B.; Vasiljevic, N.; Dimitrov, N. Metal Deposition via Electroless Surface Limited Redox Replacement. *Electrochem. Commun.* **2014**, *44*, 19.
- (24) Achari, I.; Ambrozik, S.; Dimitrov, N. Electrochemical Atomic Layer Deposition of Pd Ultra-Thin Films by Surface Limited Redox Replacement of Underpotentially Deposited H in a Single Cell. *J. Phys. Chem. C* **2017**, *121*, 4404.
- (25) Budevski, E.; Staikov, G.; Lorenz, W. J. In *Electrochemical Phase Formation and Growth*; Alkire, R.C. et al., Ed.; VCH: Berlin, 1996; p 97.

- (26) Yuan, Q.; Tripathi, A.; Slavkovic, M.; Brankovic, S. R. Lead Underpotential Deposition on Pt-submonolayer Modified Au(111). *Z. Phys. Chem.* **2012**, *226*, 965.
- (27) Prentice, G. *Electrochemical Engineering Principles*; Prentice Hall: Upper Saddle River, NJ, 1991; p 29.
- (28) Budevski, E.; Staikov, G.; Lorenz, W. J. In *Electrochemical Phase Formation and Growth*; Alkire, R.C. et al., Ed.; VCH: Berlin 1996; p 41.
- (29) Green, M. P.; Hanson, K. J.; Carr, R.; Lindau, I. STM Observations of the Underpotential Deposition and Stripping of Pb on Au(111) under Potential Sweep Conditions. *J. Electrochem. Soc.* **1990**, *137*, 3493.
- (30) Shin, J. W.; Bertocci, U.; Stafford, G. R. Stress Response to Surface Alloying and Dealloying during Underpotential Deposition of Pb on (111) Textured Au. *J. Phys. Chem. C* **2010**, *114*, 7926.
- (31) Jones, D. A. *Principles and Prevention of Corrosion*, 2nd ed.; Prentice Hall, Upper Saddle River, NJ, 1992; p 75.
- (32) Vasilic, R.; Vasiljevic, N.; Dimitrov, N. Open Circuit Stability of Underpotentially Deposited Pb Monolayer on Cu(111). *J. Electroanal. Chem.* **2005**, *580*, 203.
- (33) Fontana, M. G. *Corrosion Engineering*, 3rd. ed.; McGraw-Hill: New York, 1985; p 457.
- (34) Zeradjanin, A. R.; Grote, J. P.; Polymeros, G.; Mayrhofer, K. J. J. A Critical Review on Hydrogen Evolution Electrocatalysis: Re-exploring the Volcano-relationship. *Electroanalysis* **2016**, *28*, 2256.
- (35) Trasatti, S. *Proceedings of the Symposium on Electrocatalysis*; Grady, W. E. O. Q.; Ross, P. N., Will, F. G. Eds.; The Electrochemical Society Proceedings Series; Pennington, NJ, 1982; p 73.
- (36) Swathirajan, S.; Bruckenstein, S. Thermodynamics and Kinetics of Underpotential Deposition of Metal Monolayers on Polycrystalline Substrates. *Electrochim. Acta* **1983**, *28*, 865.
- (37) Trasatti, S. Work Function, Electronegativity, and Electrochemical Behaviour of Metals: II. Potentials of Zero Charge and Electrochemical Work Functions. *J. Electroanal. Chem. Interfacial Electrochem.* **1971**, *33*, 351.
- (38) Kolb, D. M. *Physical and Electrochemical Properties of Metal Monolayers on Metallic Substrates in Advances in Electrochemical Engineering*; Gerischer, H., Tobias, W., Eds.; Wiley & Sons: New York, 1978), p 125.
- (39) Kiselev, V. F.; Krylov, O. V. *Adsorption and Catalysis on Transition Metals and Their Oxides*; Springer-Verlag: New York, 1989; p 5.
- (40) Conway, B. E. *Theory and Principles of Electrode Processes*; The Ronald Press Company: New York, 1965; p 170.
- (41) Conway, B. E.; Bockris, J. O'M. Electrolytic Hydrogen Evolution Kinetics and Its Relation to the Electronic and Adsorptive Properties of the Metal. *J. Chem. Phys.* **1957**, *26*, 532.
- (42) Wynblatt, P. A Calculation of the Surface Energies of fcc Transition Metals. *Surf. Sci.* **1984**, *136*, L51.
- (43) Bauer, E. Phänomenologische Theorie der Kristallabscheidung an Oberflächen I. *Z. Kristallogr.* **1958**, *110*, 372.